J. Membrane Biol. 150, 57–69 (1996)

The Journal of
Membrane
Biology

Modeling Facilitative Sugar Transporters: Transitions Between Single and Double Ligand Occupancy of Multiconformational Channel Models Explain Anomalous Kinetics

J.A. Hernández[1], **J. Fischbarg**[2], **J.C. Vera**[3]

[1]Sección Biofísica, Facultad de Ciencias, Universidad de la República, 11200 Montevideo, Uruguay
[2]Departments of Physiology & Cellular Biophysics, and Ophthalmology, College of Physicians and Surgeons, Columbia University, New York, NY 10032
[3]Program in Molecular Pharmacology and Therapeutics, Memorial Sloan Kettering Cancer Center, New York, NY 10021

Received: 12 April 1995/Revised: 28 August 1995

Abstract. The four-state simple carrier model (SCM) is employed to describe ligand translocation by diverse passive membrane transporters. However, its application to systems like facilitative sugar transporters (GLUTs) is controversial: unidirectional fluxes under zero-trans and equilibrium-exchange experimental conditions fit a SCM, but flux data from infinite-cis and infinite-trans experiments appear not to fit the same SCM. More complex kinetic models have been proposed to explain this ''anomalous'' behavior of GLUTs, but none of them accounts for all the experimental findings. We propose an alternative model in which GLUTs are channels subject to conformational transitions, and further assume that the results from zero-trans and equilibrium-exchange experiments as well as trans-effects corresponds to a single-occupancy channel regime, whereas the results from the infinite-cis and infinite-trans experiments correspond to a regime including higher channel occupancies. We test the plausibility of this hypothesis by studying a kinetic model of a two-site channel with two conformational states. In each state, the channel can bind the ligand from only one of the compartments. Under single-occupancy, for conditions corresponding to zero-trans and equilibrium-exchange experiments, the model behaves as a SCM capable of exhibiting trans-stimulations. For a regime including higher degrees of occupancy and infinite-cis and infinite-trans conditions, the same channel model can exhibit a behavior qualitatively similar to a SCM, albeit with kinetic parameters different from those for the single-occupancy regime. Numerical results obtained with our model are consistent with available experimental data on facilitative glucose transport across erythrocyte membranes. Hence, if GLUTs are multiconformational channels, their particular kinetic properties can result from transitions between single and double channel occupancies.

Key words: Sugars — Facilitators — Carriers — Channels — Pores — Kinetic models

Introduction

Facilitative transporters or organic ligands are widely distributed among biological membranes. They are complex integral membrane proteins that perform translocation of ligands via mechanisms usually involving conformational transitions of the macromolecule. The four-state ''simple carrier'' model (SCM) is the most elementary scheme to describe the kinetics of facilitative transport mediated by conformational changes of the protein (Stein, 1986, pp. 231–242). Facilitative sugar transporters (GLUTs) play crucial roles in the physiology of animal cells, and have been the subject of intense research. The overwhelming amount of data on structural and functional aspects of the GLUTs has been summarized in diverse reviews (Wheeler & Hinkle, 1985; Baly & Horuk, 1988; Carruthers, 1990; Baldwin, 1993; Gould & Holman, 1993; Mueckler, 1994). The kinetic properties of the GLUTs have been classically interpreted in terms of the SCM (Widdas, 1952; Gorga & Lienhard, 1981; Appleman & Lienhard, 1985, 1989; Lowe & Walmsley, 1986; Wheeler, 1986; Walmsley, 1988; Wheeler & Whelan, 1988; Walmsley et al., 1994). However, the SCM fails to explain all the available kinetic evidence (for analysis of this

Correspondence to: J. Fischbarg

problem *see* Stein, 1986, pp. 251–255; Helgerson & Carruthers, 1987; Wheeler & Whelan, 1988; Carruthers, 1990). Thus, the results from flux measurements done under infinite-cis and infinite-trans conditions cannot be easily interpreted in terms of the same SCM that would characterize results from zero-trans and equilibrium-exchange experiments (''anomalous'' kinetic findings, *see* Stein, 1986, p. 253; Carruthers, 1990). More complex kinetic schemes have been suggested as alternatives (Lieb & Stein, 1970; Naftalin, 1970; Krupka, 1972; Baker & Widdas, 1973; Batt & Schachter, 1973; Eilam, 1975; Ginsburg, 1978; Holman, 1980). Yet, not even such models fit the totality of experimental results (Krupka & Deves, 1981; Weiser et al., 1983; Naftalin et al., 1985; Stein, 1986, pp. 253–254; Krupka, 1989; Carruthers, 1990). More recently, it has been suggested that the anomalous kinetic behavior of the glucose transporter present in erythrocytes (GLUT1) would arise from a transition between different GLUT1 oligomeric structures (Hebert & Carruthers, 1992). Evidence consistent with this view comes from the finding of allosteric behavior (Carruthers, 1991; Carruthers & Helgerson, 1991) and from structural studies (Pessino et al., 1991; Hebert & Carruthers, 1992). A model based upon these findings (Hebert & Carruthers, 1992) proposes that GLUT1 exists in two basic structural forms, a dimer and a tetramer. Each monomer in either form behaves as a typical one-site carrier (a SCM), but exhibits different kinetic properties depending on the oligomer. To explain the anomalous kinetic findings, the subunits are proposed to behave as independent SCMs in the dimer, whereas they are conformationally constrained in the tetramer. However, although this model represents a plausible proposal, it is not clear whether transitions between the different oligomeric states of GLUT1 actually occur *in situ* at the erythrocyte membrane (for discussions, *see* Baldwin, 1993; Gould & Holman, 1993; Marshall et al., 1993; Shetty et al., 1993).

Aside from kinetic considerations, the relation between the functional characteristics of GLUTs and their putative structure has also been the subject of analysis. Thus, it has been suggested that GLUTs may operate by means of inner channels undergoing conformational changes (Barnett et al., 1973, 1975). More recent kinetic and structural evidence supports this idea. Data on hydrogen-exchange (Jung et al., 1986), infrared spectroscopic analysis (Alvarez et al., 1987) and studies on water permeability (Fischbarg et al., 1990; Zhang et al., 1991) contribute to the concept that GLUTs operate by means of a hydrophilic channel, accessible both to sugar substrates and to water molecules. Indeed, the structural models proposed for GLUTs suggest the presence of an inner channel spanning the membrane (Mueckler et al., 1985; Fischbarg et al., 1993; Fischbarg & Vera, 1994). Thus, realistic models of the kinetic properties of GLUTs might need to include water-ligand interactions inside a channel subject to conformational changes. Such channel models may be extremely complex, even in the simpler case of a single-file channel (Hernández & Fischbarg, 1994). Still, complicated models involving water-ligand interactions may nevertheless behave like ligand-only models under certain conditions (Hernández & Fischbarg, 1994), thus justifying the present use of a model where only transitions involving the ligand are considered.

The purpose of this work is to advance an alternative way to interpret the kinetic properties of GLUTs. For this, we assume that these transporters operate via channels undergoing conformational transitions. Different conformational states of a transporter may be able to bind different ligands; some of the ligands can be transported but others not. Here, we only consider the case of a single ligand that can be transported (e.g., glucose). Since no complete mechanistic description can be at present advanced for GLUTs, we exemplify our approach with the analytical and numerical study of a particular simple case of a two-conformational, two-site channel model. The numerical example shown here (Appendix III) should only be considered as another argument in favor of the plausibility of the hypothesis evaluated here (*see below*), and not as a proposal of actual parameter values. The main objective of this work is to test the hypothesis that the discrepancies with the single SCM for a GLUT (''anomalous findings,'' *see above*) can be explained if the GLUT channel can be occupied by more than one ligand molecule at a time. The basic assumption to perform the analysis, and to relate it to the findings about the GLUTs, is that the results from the zero-trans, equilibrium-exchange, and trans-effects experiments can be interpreted in terms of a single-occupancy regime of the model, whereas the results from the ''infinite'' experiments (infinite-cis and infinite-trans) may require to consider higher degrees of saturation of the model. Surprisingly, this rather simple conception leads to a consistent picture in which all available results could be framed into. Some of these ideas might also apply to other facilitative transport systems exhibiting kinetic properties that do not easily fit the SCM, such as the choline transporter (Krupka & Deves, 1983).

Results

A Two-Conformational Channel Model of Facilitative Sugar Transport

Figure 1*A* shows the complete model corresponding to the two-conformational, two-site channel considered here. Each conformational state can bind a ligand *S* from only one of the two compartments (1 and 2). Since we

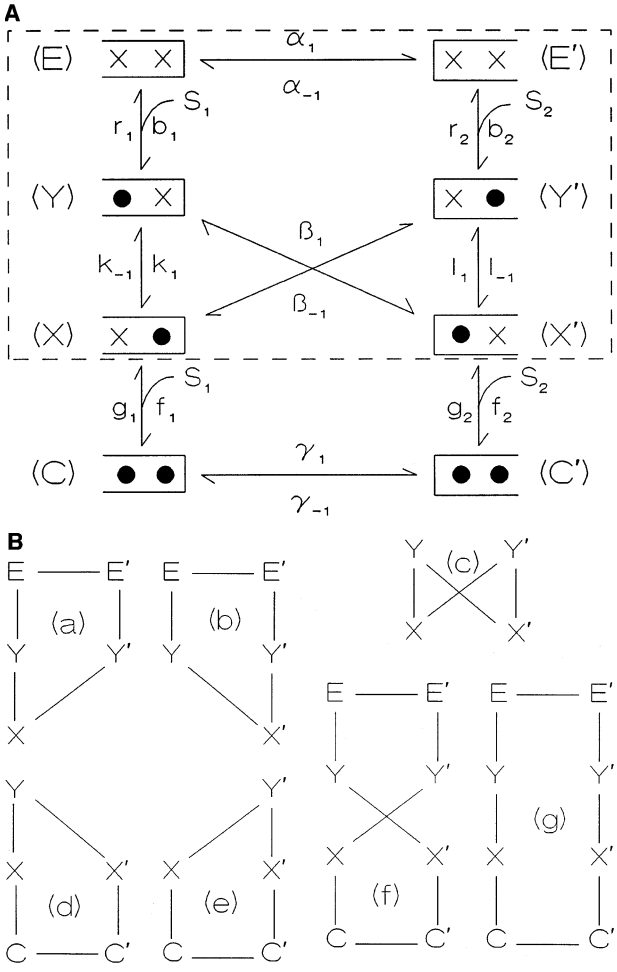

Fig. 1. (*A*) Complete state diagram of a two-conformational two-site channel that transports a ligand *S* between compartments 1 and 2. Dark circles: ligand molecules; *X:* vacant positions inside the channel. (*E*), (*E′*), (*Y*), (*Y′*), (*X*), (*X′*), (*C*), and (*C′*), are the intermediate states of the channel. S_1 and S_2 represent the ligand in compartments 1 and 2 respectively; b_1 and f_1, b_2 and f_2, are the rate constants for binding from compartments 1 and 2 respectively; r_1 and g_1, r_2 and g_2, are the rate constants for release to compartments 1 and 2 respectively; k_1, k_{-1}, l_1 and l_{-1} are the rate constants for the movement between positions inside the channel, and α_1, α_{-1}, β_1, β_{-1}, γ_1, and γ_{-1}, are the rate constants governing the conformational transitions. The region enclosed by the dashed-lined rectangle corresponds to the single-occupancy mode of operation of the model. (*B*) The cycles contained in the diagram of Fig. 1*A*.

assume that this property is independent of the presence of a ligand molecule inside the channel, the binding of a second ligand molecule to the channel is also subject to this restriction. This behavior can be interpreted in terms of the height of the activation energy barriers characterizing the binding steps to the end-positions of the channel (Läuger, 1980, 1984). Although the model of Fig. 1*A* is simple by comparison to what the actual inner channel of a transporting protein may be, it is nevertheless complex from an analytical point of view. The application of

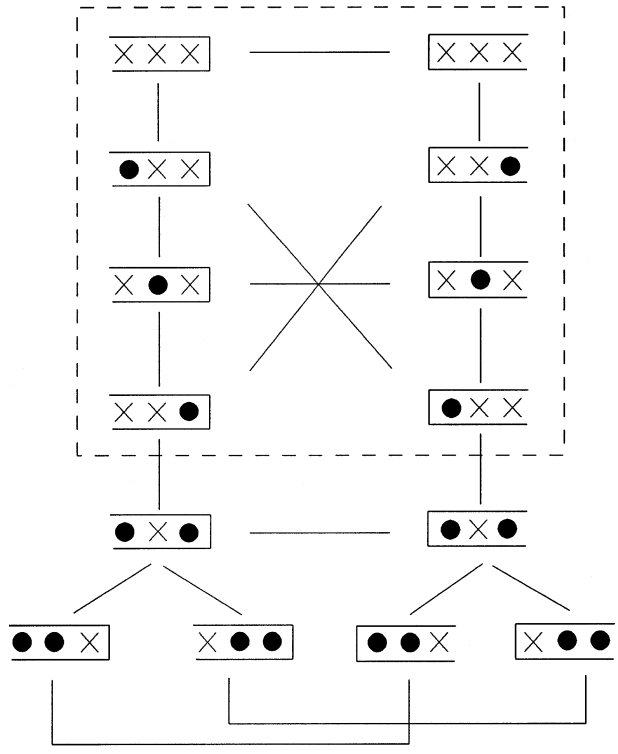

Fig. 2. A state diagram analogous to the one shown in Fig. 1*A*, but for a three-site channel. The solid lines represent actual individual transitions, not shown in detail. The dashed-line rectangle encloses the segment of the model corresponding to the single-occupancy mode of operation.

the diagram algorithm (Hill, 1977) to the analysis of the model under steady-state conditions illustrates this point. Indeed, the diagram of Fig. 1*A* contains eight channel states, and gives rise to seven cycles (Fig. 1*B*) and to more than 500 directional diagrams. In Fig. 2, we show the state diagram of a still more complex case, that of a three-site channel undergoing occupancy but, at most, two ligand molecules. In general, if n is the number of positions in the channel, and if we assume that a significant description of the transport process under the usual experimental conditions only needs to consider at most double-occupancy states, the number of states in the diagram equals $[2 + n(n + 1)]$. The increasing complexity with n is already illustrated in the diagram of Fig. 2, that contains 14 channel states.

The ''complete'' model of Fig. 1*A* results in the most general description of the example under consideration. We first analyze it for the limiting case of the single-occupancy regime, under which we derive analytical expressions for the unidirectional fluxes of *S.* We use them to derive expressions for the relevant parameters for zero-trans and equilibrium-exchange experiments, and to derive the analytical conditions determining trans-stimulation by the presence of the ligand in the trans compartment. We subsequently employ the model

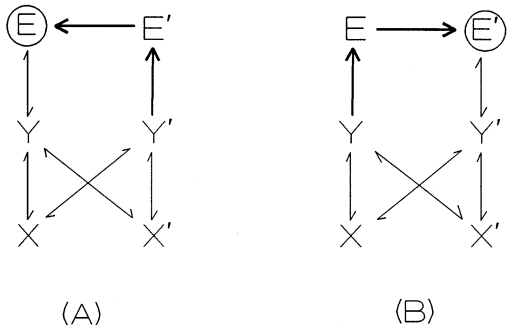

Fig. 3. (*A*) Cyclic diagram representing the unidirectional flux of *S* in the $1 \rightarrow 2$ direction determined by the single-occupancy limit of the model of Fig. 1*A*. *S* is bound by state *E* from compartment 1, and released to compartment 2 in transition $Y' \rightarrow E'$. (*B*) Similar to Fig. 3*A*, but for the $2 \rightarrow 1$ direction.

under higher saturation regimes to derive expressions for the net flux and for the unidirectional fluxes of *S*, in order to discuss infinite-cis and infinite-trans conditions respectively. In every case, the steady-state expressions are derived by means of the diagram method (Hill, 1977). Finally, we advance a numerical example (Appendix III) to illustrate the application of the model to the available experimental data for kinetic properties of GLUT1.

Low Degree of Saturation: Single-Occupancy Model

Under low saturation conditions, we assume that the transport process can be adequately described by the single-occupancy limit of the complete model of Fig. 1*A*. The kinetic condition determining this limit is given by Eq. (A16). The state diagram corresponding to the single-occupancy regime of the transporter is the one determined by cycles *a*, *b* and *c* only (Fig. 1*B*); the steady-state analysis of this situation is performed in Appendix I. Figure 3A and *B* show the cyclic diagrams used to derive the expressions for the unidirectional fluxes of *S* in the two directions. As can be seen from the inspection of Fig. 1*A*, and from the results derived in Appendix I, under the single-occupancy regime the behavior of the model is formally analogous to the SCM. The idea that channels undergoing conformational transitions may, under specific conditions, behave like carriers has already been sketched (*see*, for instance, Baker & Naftalin, 1979; Holman, 1980). Such an idea has been developed in more complete form by Läuger (1980, 1984) from the study of simple models of ionic channels. The same behavior is valid for channels with more sites; for instance, in the three-site model of Fig. 2, the single-occupancy segment (enclosed by the dashed rectangle) is formally similar to the corresponding one in the model of Fig. 1*A*, and would give rise to similar general SCM-type kinetic expressions.

We now derive the experimentally relevant parameters that characterize the kinetic properties of the unidirectional fluxes of *S* [given by Eqs. (A11*a*) and (A11*b*)] for the simple case of the single-occupancy model. We follow the analysis and notations employed by Lieb and Stein (1974; *see also* Stein, 1986, pp. 237–242). As mentioned above, we consider that Eqs. (A11) apply for the zero-trans and equilibrium-exchange experiments, and also for the effects of trans-stimulations.

For the zero-trans conditions, we set $S_2 = 0$ and $S_1 = 0$ in the expressions for v_{12} [Eq. (A11*a*)] and v_{21} [Eq. (A11*b*)] respectively. Each resulting expression follows classical Michaelis-Menten kinetics as a function of the ligand activity in the corresponding cis compartment, characterized by the following parameters:

$$V^{zt}_{12} = 1/R_{12};\ V^{zt}_{21} = 1/R_{21};$$
$$K^{zt}_{12} = KR_{00}/R_{12}, \text{ and } K^{zt}_{21} = KR_{00}/R_{21}, \qquad (1)$$

where, for the single-occupancy model under consideration, *K*, R_{12}, R_{21} and R_{00} are given by Eqs. (A12)–(A14). In Eqs. (1), V^{zt}_{12} and V^{zt}_{21} represent the maximum fluxes under zero-trans conditions in the $1 \rightarrow 2$ and $2 \rightarrow 1$ directions respectively, and K^{zt}_{12} and K^{zt}_{21} the corresponding half-saturation concentrations.

For the equilibrium-exchange condition, we set $S_1 = S_2 = S$ in either expression for the unidirectional flux [Eq. (A11*a*) or Eq. (A11*b*)]. The resulting expression follows Michaelis-Menten kinetics as a function of *S*, characterized by the following maximum flux V_{ee} and half-saturation concentration K_{ee}:

$$V_{ee} = 1/R_{ee}, \text{ and } K_{ee} = KR_{00}/R_{ee}, \qquad (2)$$

where R_{ee} is defined by Eqs. (A12)–(A14).

Since, as already mentioned, the single-occupancy portion of the model of Fig. 1*A* is formally analogous to a SCM, it can account for the phenomenon of trans-acceleration (Lieb, 1982; Stein, 1986, p. 240). There will be trans-acceleration in the $1 \rightarrow 2$ ($2 \rightarrow 1$) direction if $dv_{12}/dS_2 > 0$ ($dv_{21}/dS_1 > 0$). This requires the condition that $R_{12} > R_{ee}$ ($R_{21} > R_{ee}$) from trans-stimulation in the $1 \rightarrow 2$ ($2 \rightarrow 1$) direction (Stein, 1986, p. 240).

From the above, the results of this section totally conform to the classical kinetic properties of a SCM (Stein, 1986, pp. 237–242).

Higher Degree of Saturation: The Complete Model

Under conditions of higher degrees of saturation, the general model of Fig. 1*A* should apply. The kinetic parameters of the model determine the range of activity values of *S* for the single and double-occupancy limits [Eqs. (A16) and (A17) respectively]. Thus, the deviation from the SCM behavior characteristic of the single-

occupancy regime of the complete model would range from small perturbations to the properties of the full-saturation regime represented, in such case, by the double-occupancy limit (given by cycles *c*, *d* and *e* in Fig. 1*B*). As noted above, the steady state analysis of the relatively simple model of Fig. 1*A* is already very much involved. The technical difficulties for such analysis become particularly notorious in the derivation of explicit expressions for the unidirectional fluxes (*see*, for instance, Hill, 1989, pp. 68–84). For the illustrative purposes of this article we now assume that, under some intermediate values of the ligand activities, the behavior of the system can be adequately represented by considering cycle *g* only (Fig. 1*B*), which we analyze in Appendix II. For this case, we provide the expressions representing the flux of *S* under the infinite-cis and infinite-trans conditions. In Fig. 4, we show the cyclic diagrams used in Appendix II to derive the expressions for the unidirectional fluxes of *S*.

The net flux of *S* (taking as positive the 1 to 2 direction) is given by Eq. (A15). Under a condition intermediate between those defined by Eqs. (A16) and (A17), cycle *g* contributes significantly to this flux [Eq. (A19)]. We shall employ Eq. (A19) to deduce the behavior of such an intermediate occupancy regime under infinite-cis conditions. For the 1 to 2 direction, the net flux under infinite-cis conditions (saturating S_1) is given by

$$J_S = (2N\Pi_g)/(H_4 + H_6S_2 + H_8S_2^2) \quad (3)$$

where H_4, H_6 and H_8 are defined by Eqs. (A21)–(A23).

The behavior of J_S as a function of S_2 in Eq. (3) is characterized by a maximum flux V^{ic}_{12} (corresponding to $S_2 = 0$) and a half-saturation concentration K^{ic}_{12} given by

$$V^{ic}_{12} = 2N\Pi_g/H_4;\ K^{ic}_{12} = [(H_6^2 + 4H_4H_8)^{1/2} - H_6]/2H_8 \quad (4a)$$

Under experimental conditions for which the terms in S_2^2 can be neglected, K^{ic}_{12} will be given by $K^{ic}_{12} = H_4/H_6$. Analogous considerations would lead us to conclude that

$$V^{ic}_{21} = 2N\Pi_g/H_5;\ K^{ic}_{21} = [(H_7^2 + 4H_5H_8)^{1/2} - H_7]/2H_8 \quad (4b)$$

Where H_5 and H_7 are defined by Eqs. (A21)–(A23).

Similar to the previous case, if terms in S_1^2 can be neglected, K^{ic}_{21} will be given by $K^{ic}_{21} = H_5/H_7$. Thus, under infinite-cis conditions the model exhibits a qualitative behavior similar to that of a SCM (*see*, for instance, Stein, 1986, pp. 239–240), although with kinetic parameters different to the ones corresponding to the single-occupancy case.

The total unidirectional fluxes determined by cycle *g* are given by Eqs. (A25)–(A26). Under infinite-trans conditions in the $1 \rightarrow 2$ direction, S_2 is present in saturating activities. In this case, the corresponding unidirectional flux [Eq. (A25*a*)] becomes

$$v_{12} = (N\Pi_g S_1^2)/Z_0 + Z_1S_1 + Z_2S_1^2 + Z_3S_1^3) \quad (5)$$

where

$$\begin{aligned}
Z_0 &= (\alpha_{-1}k_{-1}l_1r_1r_2GH_5)/(\gamma_{-1}g_1k_{-1}l_{-1}r_1b_2f_2)\\
Z_1 &= [\alpha_{-1}\gamma_1g_2l_1r_2(k_1 + r_1)f_1H_5 + \alpha_{-1}k_{-1}l_1r_1r_2GH_7]/\\
&\quad (\gamma_{-1}g_1k_{-1}l_{-1}r_1b_2f_2)\\
Z_2 &= [\alpha_{-1}\gamma_1g_2l_1r_2(k_1 + r_1)f_1H_7 + \alpha_{-1}k_{-1}l_1r_1r_2G\ H_8]/\\
&\quad (\gamma_{-1}g_1k_{-1}l_{-1}r_1b_2f_2)\\
Z_3 &= [\alpha_{-1}\gamma_1g_2l_1r_2(k_1 + r_1)\ f_1H_8/(\gamma_{-1}g_1k_{-1}l_{-1}r_1b_2f_2) \quad (6)
\end{aligned}$$

with G, H_5, H_7 and H_8 defined by Eqs. (A21)–(A23).

For the interval of experimental values of S_1 for which terms in S_1^3 can be neglected, Eq. (5) exhibits saturation kinetics characterized by a maximum flux V^{it}_{12} and a half-saturation concentration K^{it}_{12} given by

$$V^{it}_{12} = N\Pi_g/Z_2;\ K^{it}_{12} = (Z_1/2Z_2) \pm [(Z_1^2 + 4Z_0Z_2)^{1/2}]/2Z_2 \quad (7a)$$

Analogous considerations for the $2 \rightarrow 1$ direction would lead to

$$V^{it}_{21} = N\Pi_g/Z'_2;\ K^{it}_{21} = (Z'_1/2Z'_2) \pm [(Z'^2_1 + 4Z'_0Z'_2)^{1/2}]/2Z'_2 \quad (7b)$$

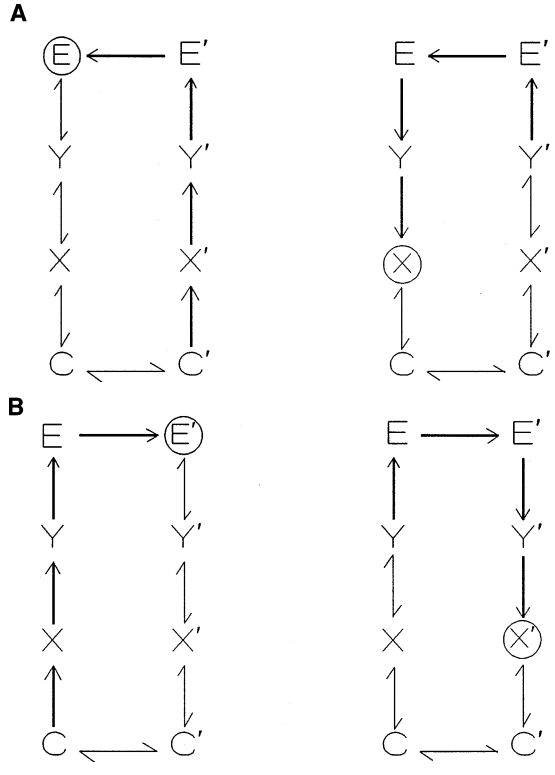

Fig. 4. (*A*) Cyclic diagrams representing the two forms of unidirectional fluxes in the $1 \rightarrow 2$ direction, for the model represented by cycle *g* only. In the diagram on the left, *S* is bound by intermediate form *E* and released by *C′*; in the diagram on the right, *S* is bound by intermediate form *X* and released by *Y′*. (*B*) Cyclic diagrams analogous to Fig. 4*A*, but for the $2 \rightarrow 1$ direction.

Table 1. Expressions derived for the kinetic parameters under the single-occupancy limit and under the regime represented by cycle g.

(A) SINGLE-OCCUPANCY LIMIT (SCM behavior)	
Maximum unidirectional flux	Half-saturation concentration
$V^{zt}_{12} = 1/R_{12}$	$K^{zt}_{12} = KR_{00}/R_{12}$
$V^{zt}_{21} = 1/R_{21}$	$K^{zt}_{21} = KR_{00}/R_{21}$
$V_{ee} = 1/R_{ee}$	$K_{ee} = KR_{00}/R_{ee}$,
(B) CYCLE g	
Maximum net flux	Half-saturation concentration
$V^{ic}_{12} = N\Pi_g/H_4$	$K^{ic}_{12} = [(H_6^2 + 4H_4H_8)^{1/2} - H_6]/2H_8$
$V^{ic}_{21} = N\Pi_g/H_5$	$K^{ic}_{21} = [(H_7^2 + 4H_5H_8)^{1/2} - H_7]/2H_8$
Maximum unidirectional flux	
$V^{it}_{12} = N\Pi_g/Z_2$	$K^{it}_{12} = (Z_1/2Z_2) \pm [(Z_1^2 + 4Z_0Z_2)^{1/2}]/2Z_2$
$V^{it}_{21} = N\Pi_g/Z'_2$	$K^{it}_{21} = (Z'_1/2Z'_2) \pm [(Z'^2_1 + 4Z'_0Z'_2)^{1/2}]/2Z'_2$

zt: zero-trans; *ee:* equilibrium-exchange; Kinetic restriction: $R_{00} + R_{ee} = R_{12} + R_{21}$ [Eqs. (A12)–(A14)]; K, R_{00}, R_{ee}, R_{12}, and R_{21} giuven by Eqs. (A12)–(A14).
ic: infinite-cis; it: infinite trans; Kinetic restriction: not determined; Π_g given by Eq. (A24); H4, H5, H6, H7, and H8 given by Eqs. (A21)–(A23); Z_0, Z_1, Z_2, Z'_0, Z'_1, and Z'_2 given by Eqs. (6) and (8).

where

$$Z'_0 = (\alpha_1 k_{-1} l_1 r_1 r_2 G H_4)/(\gamma_1 g_2 k_1 l_1 r_2 b_1 f_1)$$
$$Z'_1 = [\alpha_1\gamma_{-1} g_1 k_{-1} r_1 (l_{-1} + r_2) f_2 H_4 + \alpha_1 k_{-1} l_1 r_1 r_2\, G\, H_6]/(\gamma_1 g_2 k_1 l_1 r_2 b_1 f_1)$$
$$Z'_2 = [\alpha_1\gamma_{-1} g_1 k_{-1} r_1 (l_{-1} + r_2) f_2 H_6 + \alpha_1 k_{-1} l_1 r_1 r_2 G H_8]/(\gamma_1 g_2 k_1 l_1 r_2 b_1 f_1) \quad (8)$$

with G, H_4, and H_8 defined by Eqs. (A21)–(A23).

A relation analogous to Eq. (A13) should also apply for cycle g, which would restrict the explicit solutions for K^{it}_{12} and K^{it}_{21}, but it is not analyzed here.

In principle, V^{it}_{12} and V^{it}_{21} [Eqs. (7*a*) and (7*b*)] appear to be different for the model under consideration (they should be equal for a strict SCM, *see* Stein, 1986, p. 239), although it is difficult to predict how significant this difference would be. Actual experiments have indeed failed to determine similar values for the maximum influx and efflux values for glucose under infinite-trans conditions (Lacko, Wittke & Geck, 1973; Baker & Naftalin, 1979; Wheeler, 1986). Similarly to the infinite-cis conditions, the qualitative behavior of the unidirectional fluxes corresponding to cycle g under infinite-trans conditions may therefore be similar to that of a SCM.

Discussion

Since $R_{00} = R_{12} + R_{21} - R_{ee}$ [Stein, 1986, p. 239; *see also* Eqs. (A12)–(A14)], the zero-trans and equilibrium-exchange experiments allow one to obtain numerical values for all the experimentally relevant parameters of a SCM, R_{12}, R_{21}, R_{ee}, R_{00}, and K. If a facilitative transporter operates as a SCM under all conditions, these parameters can also be calculated in an independent fashion, from the experimental determinations of V^{ic}_{12}, K^{ic}_{12}, V^{ic}_{21}, K^{ic}_{21}, V^{it}_{12}, K^{it}_{12}, V^{it}_{21} and K^{it}_{21} (Stein, 1986, p. 239). In order to relate our results to these procedures, we now refer to Tables 1*A* and *B*, where we show a summary of the expressions derived here. Table 1*A* shows the parameters for the single-occupancy regime of the complete model of Fig. 1*A*, corresponding to the fluxes under zero-trans and equilibrium-exchange conditions. Table 1*B* shows the parameters for the higher occupancy model represented by cycle g (Fig. 1*B*), corresponding to the fluxes under infinite-cis and infinite-trans conditions. As mentioned above, if the values obtained for R_{12}, R_{21}, R_{ee}, R_{00}, and K from the experimental determinations of the maximum fluxes and half-saturation concentrations characterizing infinite-cis and infinite-trans experiments coincide with those determined under zero-trans and equilibrium-exchange conditions, the kinetic behavior of the system can be described by a single SCM. However, if the infinite-cis and infinite-trans experiments imply conditions of higher degrees of saturation, as in the situation exemplified here, there will be in general discrepancies (''anomalous'' kinetic findings) between the values determined for the relevant SCM parameters from the two sets of data. This is a consequence of the different kinetic parameters governing the single-occupancy and higher-occupancy regimes, made explicit in the expressions shown in Table 1*A* and *B*.

Appendix III offers a numerical example of the concepts commented above. The criteria and methodology employed to determine the particular set of values chosen for the rate constants governing the model of Fig. 1*A* are detailed in that section, and basically rest on the consistency with a variety of available experimental data such as those summarized by Baldwin (*ibid*, 1993). In general, the kinetic parameters calculated here (Tables 2 and 3) for the single-occupancy limit of the model in Fig. 1*A* are in reasonable agreement with the experimental values for facilitated glucose transport across erythrocyte membranes at 0°C (Lowe & Walmsley, 1986; Wheeler &

Table 2. Numerical values obtained for the kinetic parameters corresponding to the single-occupancy limit of the model in Fig. 1*A*

(A) Experimentally relevant parameters			
$K = 0.107$			
$R_{12} = 13.19$			$R_{21} = 183.90$
$R_{ee} = 2.42$			$R_{00} = 194.67$
(*K:* mM; *R: lt s* mmol^{-1})			
(B) Maximal velocities and apparent K_m values			
V_{max}	Calculated		
(mmol lt^{-1} s^{-1})	value	Experimental value	Experimental conditions
V^{zt}_{12}	0.0760	0.071 (*a*); 0.150 (*b*)	zero-trans efflux
V^{zt}_{21}	0.0054	0.0055 (*a*)	zero-trans influx
V_{ee}	0.4133	0.563 (*a*)	equilibrium exchange
Apparent K_m	Calculated		
(mM)	value	Experimental value	Experimental conditions
K^{zt}_{12}	1.58	1.64 (*a*); 3.4 (*b*)	zero-trans efflux
K^{zt}_{21}	0.11	0.145 (a)	zero-trans influx
K_{ee}	8.60	12.8 (a)	equilibrium exchange

(*a*) Lowe & Walmsley, 1986; (*b*) Wheeler, 1986

Table 3. Kinetic parameters corresponding to the single occupancy limit and cycle$_g$ of the model in Fig. 1A. comparison with experimental values

V_{max} (mmol lt^{-1} s^{-1})	Single occupancy regime	Double occupancy regime (cycle *g*)	Experimental values	Experimental conditions
V^{ic}_{12}	0.0760	0.1540	0.143 (*a*)	inf.-cis efflux
V^{ic}_{21}	0.0054	0.0109	0.0051 (*d*)	inf.-cis influx
V^{it}_{12}	0.4133	0.5320	0.73 (*c*, *d*)	inf.-trans efflux
V^{it}_{21}	0.4133	0.1920	0.21 (*c*, *d*)	inf.-trans influx
Apparent K_m (mM)	Single occupancy regime	Double occupancy regime (cycle *g*)	Experimental values	Experimental conditions
K^{ic}_{12}	0.58	1.52	0.39 (*a*)	inf.-cis efflux
K^{ic}_{21}	8.13	4.57	4.4 (*b*); 14.6 (*d*)	inf.-cis influx
K^{it}_{12}	8.13	7.02	8.7 (*c*, *d*)	inf.-trans efflux
K^{it}_{21}	0.58	1.05	0.65 (*c*, *d*)	inf.-trans influx

(*a*) Baker & Naftalin, 1979; (*b*) Carruthers & Melchior, 1985; (c) Wheeler, 1986; (d) Wheeler & Whelan, 1988.

Whelan, 1988; Carruthers, 1990; Baldwin, 1993). In addition, in Fig. 5 we show the concentration-dependence of ligand influx and efflux values obtained with the expressions for cycle *g* (Fig. 4) under infinite-cis and infinite-trans conditions. The plots in this figure show what the results of these experiments would be if cycle *g* represented the only kinetic mode of operation of the transport system described in Fig. 1*A*, to the exclusion of a SCM (single-occupancy) regime. Of course, cycle *g* is not likely to represent the sole regime of the transporter under infinite-cis and infinite-trans conditions. However, the plots shown in Fig. 5 give us an idea of how these conditions may alter the kinetic parameters when added to a prevailing SCM-like regime (that is, modifying the values shown in the single-occupancy column of Table 3). As mentioned above, the main idea underlying this analysis is that under the ''infinite'' conditions the appearance of higher-occupation regimes perturbs, to a variable extent, the basic SCM-like behavior of the transporting system. We will now discuss these effects by comparing the values derived for the kinetic parameters under the SCM-like regime with the ones determined from the curves shown in Fig. 5 corresponding to the double-occupancy regime characteristic of cycle *g*, and with actual experimental results (Wheeler & Whelan, 1988; Carruthers, 1990; Baldwin, 1993). These values are summarized in Table 3.

In what follows, the values inside the parenthesis corresponds to the single and double-occupancy (cycle *g*) regimes, respectively; values are those in Table 3. Under infinite-cis-conditions, the effect of cycle *g* on the ligand efflux would be to increase the maximum velocity ($V^{ic}_{12} = 0.076$ and 0.154 mmol lt^{-1} s^{-1}) and to increase the apparent K_m (as calculated: $K^{ic}_{12} = 0.58$ and 1.52

mM). Actual experiments have revealed values similar to the V^{ic}_{12} and somewhat smaller than the K^{ic}_{12} determined under cycle *g* ($V^{ic}_{12} = 0.143$ mmol lt^{-1} s^{-1} and $K^{ic}_{12} =$ 0.39 mM, Baker & Naftalin, 1979). Under the same conditions, the effect of cycle *g* on the ligand influx is to increase the maximum velocity (as calculated: $V^{ic}_{21} =$ 0.0054 and 0.0109 mmol lt^{-1} s^{-1}) and to lower the apparent K_m (as calculated: $K^{ic}_{21} = 8.13$ and 4.57 mM). Experimental data of glucose influx under infinite-cis conditions are particularly contradictory, especially concerning determinations of the apparent K_m, which has given rise to the view that GLUTs exhibit an ''anomalous'' kinetic behavior. For instance (Table 3), experimental values may range from $K^{ic}_{21} = 14.6$ mM (Wheeler & Whelan, 1988, which is in line with the kinetic behavior of GLUT1 being that of a classical SCM), to K^{ic}_{21} = 4.4 mM (Carruthers & Melchior, 1985, which in the context of the rest of the experimental results can only be explained by a behavior more complex than that of a SCM). Fittingly, the value of K^{ic}_{21} obtained in our simulation under the exclusive-cycle-*g* regime is similar to the latter experimental value. Together with the consistency between the results of the simulations performed here and the experimental data, this fact constitutes an interesting argument in favor of the mechanism suggested here to explain the anomalous behavior of GLUTs.

Under infinite-trans conditions, the effect of cycle *g* on the ligand efflux is not significant in the range of ligand concentrations evaluated here ($V^{it}_{12} = 0.4133$ and 0.5320 mmol lt^{-1} s^{-1}; $K^{it}_{12} = 8.13$ and 7.02 mM; Table 3), except for the appearance of curve-sigmoidicity, due to the presence of terms in S_1^2 in Eq. (5). For higher ligand concentrations, the curve should reveal inhibition by S_1, due to the presence of terms in S_1^3 in the denominator of that equation. Under the same conditions, the effect on the ligand influx is analogous to the effect on the efflux, although for a lower range of concentrations (of S_2 in this case). Thus, inhibition by S_2 appears rather early in the plots. In addition, the kinetic parameters determined for the single-occupancy limit and for the exclusive-cycle-*g* regime are not very different ($V^{it}_{21} = 0.4133$ and 0.1920 mmol lt^{-1} s^{-1}; $K^{it}_{21} = 0.58$ and 1.05 mM, Table 3). Both for the efflux and the influx, these simulations are in good agreement with experimental determinations (efflux: $V^{it}_{12} = 0.73$ mmol lt^{-1} s^{-1} and $K^{it}_{12} = 8.7$ mM; influx: $V^{it}_{21} = 0.21$ mmol lt^{-1} s^{-1} and $K^{it}_{21} = 0.65$ mM; Wheeler, 1986; Wheeler & Whelan, 1988, Table 3). It is interesting to note, in particular, that cycle *g* yields a better approximation (0.53 and 0.19 mmol lt^{-1} s^{-1}, Table 3) to actual experimental values of V^{it}_{12} and V^{it}_{21} (0.73 and 0.21 mmol lt^{-1} s^{-1}, Table 3) than either our current (0.4133 and 0.4133 mmol lt^{-1} s^{-1}, Table 3) or another previous simulation (0.43 and 0.43 mmol lt^{-1} s^{-1}, Wheeler & Whelan, 1988) which assume exclusive SCM behavior. Due to the approximate nature of the present analysis, it is not possible to predict here to what extent the sigmoidicity and inhibition-by-substrate, which represent other characteristics of the infinite-trans curves corresponding to cycle *g*, could become evident in the actual experimental curves.

Taken together, these numerical results are quite consistent with the experimental findings, and therefore constitute an argument in favor of the plausibility of the mechanism proposed here to explain the anomalous kinetic properties of GLUTs. The analytical and numerical studies commented above suggest a possible explanation of contradictory experimental results by simply assuming that GLUTs consist of multisite channels undergoing conformational transitions allowing them to bind more than one ligand molecule at a time. The nonideal kinetic behavior of GLUT1 is revealed especially in the time-course determination of glucose influx under infinite-cis conditions (Wheeler & Whelan, 1988), for which the experimental curves cannot be fitted by a curve obtained from a SCM with a single apparent K_m. If the mechanism proposed here turns out to be appropriate, the explanation of this phenomenon would be that, as glucose is taken up by the transporters from the high-concentration extracellular compartment, the transport regime starts in SCM mode but gradually shifts to more complex regimes involving higher-occupancy states. Also in favor of this idea is the fact that, for the time-course experiments under infinite-cis conditions, the erythrocytes are usually pre-equilibrated at low concentrations of glucose, which would dictate initial conditions where only empty or single-occupancy states of the transporter would be present. An alternative explanation of the time-course experiment by means of the two-oligomer model of GLUT1 (Hebert & Carruthers, 1992) should, for instance, require that during the period of time corresponding to the study and under constant experimental conditions, except for the accumulation of glucose in the erythrocyte, the transporter gradually converts from the dimeric, SCM-like form, to the more complex allosteric tetramer.

Besides the kinetic aspects discussed above, other arguments in favor of the mechanism proposed here come from structural considerations. The multiconformational channel model represents a more realistic mechanism to account for the transport processes mediated by complex membrane proteins than the classical but simplistic four-state SCM (Hernández & Fischbarg, 1994). Thus, contrary to the case of a classical one-site SCM, a two-conformational channel model can be employed to account for ligand-water interactions inside the channel and still retain a kinetic behavior similar to that of a SCM (Hernández & Fischbarg, 1994). The present view that some facilitative transporters of the type of the GLUTs behave as multifunctional systems (Sofue et al., 1992; Vera et al., 1993; Fischbarg & Vera, 1995), mediating the passage across membranes of diverse species

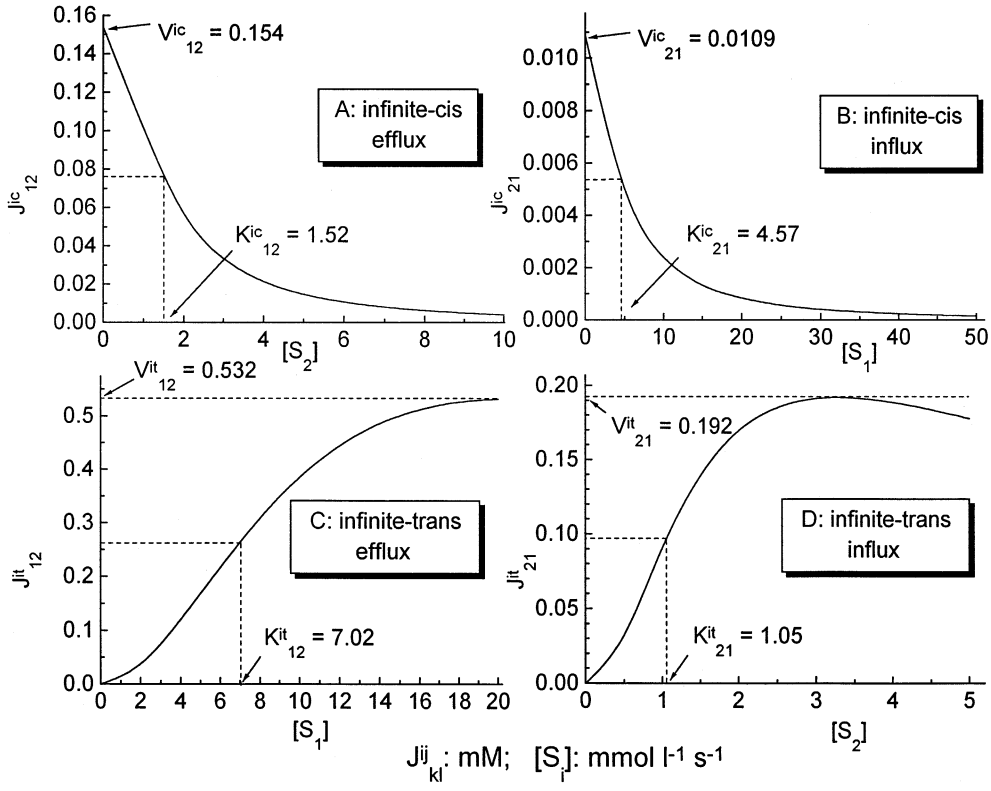

Fig. 5. Plots of the ligand flux (mmol lt^{-1} s^{-1}) as a function of the corresponding ligand concentration (mM), under infinite-cis and infinite-trans conditions, and for cycle *g* only. (*A*) $J^{ic}{}_{12}$: infinite-cis efflux, using Eq. (3); (*B*) $J^{ic}{}_{21}$: infinite-cis influx, using the version of Eq. (3) corresponding to S_1; (*C*) $J^{it}{}_{12}$: infinite-trans efflux, using Eq. (5); (*D*) $J^{it}{}_{21}$: infinite-trans influx; using the version of Eq. (5) corresponding to S_2. The kinetic parameters shown in the panels were directly obtained from the curves. They were: *V:* maximum flux, mmol lt^{-1} s^{-1}; *K:* ligand concentration corresponding to one half of the maximum flux, mM.

including water, further supports the idea that a mechanism more complex than a SCM is in operation. To summarize, the analytical results obtained in this work for a simple example of a multiconformational channel model confirm that, under the single-occupancy regime, the kinetic behavior of the model is indistinguishable from that of a SCM. Such regime has been assumed here to constitute the fundamental mode of operation of a facilitative transporter of the type of the GLUTs under zero-trans and equilibrium-exchange conditions, and for the studies of trans-stimulations. The SCM behavior of the single-occupancy regime thus determines consistent properties for the experimentally relevant parameters (Stein, 1986, p. 239). For higher degrees of occupancy, the multiconformational channel model studied here can exhibit complex kinetics. For a situation intermediate between the low and high saturation regimes and under infinite-cis and infinite-trans conditions, the model can qualitatively behave in a manner similar to that of a SCM. If our assumption of a transition from single to higher occupancy regimes is correct, the relevant kinetic parameters determined from this last set of experiments will show discrepancies with those determined under zero-trans and equilibrium-exchange conditions. The main conclusion of this work is therefore that, for facilitative transporters with kinetic behaviors that do not easily fit a SCM, as could be the case of GLUTs, their properties may be explained by a multisite multiconformational channel model capable of displaying higher than single ligand occupancies.

This work was supported by National Institutes of Health Grant EY008918, and in part by National Institutes of Health Grant CA08748 and by Research to Prevent Blindness (RPB). JAH was supported by a Fulbright Commission Award and by an RPB Travel Fellowship, and was on leave from the Universidad de la República, Uruguay.

References

Alvarez, J., Lee, D.C., Baldwin, S.A., Chapman, D. 1987. Fourier transform infrared spectroscopic study of the structure and conformational changes of the human erythrocyte glucose transporter. *J. Biol. Chem.* **262:**3502–3509

Appleman, J.R., Lienhard, G.E. 1985. Rapid kinetics of the glucose transporter from human erythrocytes. Detection and measurement of a half-turnover of the purified transporter. *J. Biol. Chem.* **260:**4575–4578

Appleman, J.R., Lienhard, G.E. 1989. Kinetics of the purified glucose transporter. Direct measurement of the rates of interconversion of transporter conformers. *Biochemistry* **28:**8221–8227

Baker, G.F., Naftalin, R.J. 1979. Evidence of multiple operational affinities for D-glucose inside the human erythrocyte membrane. *Biochim. Biophys. Acta* **550:**474–484

Baker, G.F., Widdas, W.F. 1973. The asymmetry of the facilitated transfer system for hexoses in human red cells and the simple kinetics of a two compartment model. *J. Physiol.* **231:**143–165

Baldwin, S.A. 1993. Mammalian passive glucose transporters: members of an ubiquitous family of active and passive transport proteins. *Biochim. Biophys. Acta* **1154:**17–49

Baly, D.L., Horuk, R. 1988. The biology and biochemistry of the glucose transporter. *Biochim. Biophys. Acta* **947:**571–590

Barnett, J.E.G., Holman, G.D., Chalkley, R.A., Munday, K.A. 1975. Evidence for two asymmetric conformational states in the human erythrocyte sugar-transport system. *Biochem. J.* **145:**417–429

Barnett, J.E.G., Holman, G.D., Munday, K.A. 1973. An explanation of the asymmetric binding of sugars to the human erythrocyte sugar-transport systems. *Biochem. J.* **135:**539–541

Batt, E.R., Schachter, D. 1973. Transport of monosaccharides. I. Asymmetry in the human erythrocyte mechanism. *J. Clin. Invest.* **52:**1686–1697

Britton, H.G. 1977. Calculation of steady-state rate equations and the fluxes between substrates and products in enzyme reactions. *Biochem. J.* **161:**517–526

Carruthers, A. 1990. Facilitated diffusion of glucose. *Physiol. Rev.* **70:**1135–1176

Carruthers, A. 1991. Mechanisms for the facilitated diffusion of substrates across cell membranes. *Biochemistry* **30:**3898–3906

Carruthers, A., Helgerson, A.L. 1991. Inhibition of sugar transport produced by ligands binding at opposite sides of the membrane. Evidence of simultaneous occupation of the carrier by maltose and cytochalasin B. *Biochemistry* **30:**3907–3915

Carruthers, A., Melchior, D.L. 1985. Transport of α- and β-D-glucose by the intact human red cell. *Biochemistry* **24:**4244–4250

Eilam, Y. 1975. Two carrier models for mediated transport. II. Glucose and galactose equilibrium exchange experiments in human erythrocytes as a test for several two-carrier models. *Biochim. Biophys. Acta* **401:**364–369

Fischbarg, J., Cheung, M., Czegledy, F., Li, J., Iserovich, P., Kuang, K., Hubbard, J., Garner, M., Rosen, O.M., Golde, D.W., Vera, J.C. 1993. Evidence that facilitative glucose transporters may fold as beta-barrels. *Proc. Natl. Acad. Sci. USA* **90:**11658–11662

Fischbarg, J., Kuang, K., Vera, J.C., Arant, S., Silverstein, S.C., Loike, J., Rosen, O.M. 1990. Glucose transporters serve as water channels. *Proc. Natl. Acad. Sci. USA* **87:**3244–3247

Fischbarg, J., Vera, J.C. 1995. Multifunctional transporter models: lessons from the transport of water, sugar, and ring compounds by GLUTs. *Am. J. Physiol.* **268:**C1077–C1089

Ginsberg, H. 1978. Galactose transport in human erythrocytes. The transport mechanism is resolved into two simple asymmetric antiparallel carriers. *Biochim. Biophys. Acta* **506:**119–135

Gorga, F.R., Lienhard, G.E. 1981. Equilibria and kinetics of ligand binding to the human erythrocyte glucose transporter. Evidence for an alternating conformation model for transport. *Biochemistry* **20:**5108–5113

Gould, G.W., Holman, G.D. 1993. The glucose transporter family: structure, function and tissue-specific expression. *Biochem. J.* **295:**329–341

Hebert, D.N., Carruthers, A. 1992. Glucose transporter oligomeric structure determines transporter function. Reversible redox-dependent interconversions of tetrameric and dimeric GLUT1. *J. Biol. Chem.* **267:**23829–23838

Helgerson, A.L., Carruthers, A. 1987. Equilibrium ligand binding to the human erythrocyte sugar transporter. Evidence for two sugar-binding sites per carrier. *J. Biol. Chem.* **262:**5464–5475

Hernández, J.A., Fischbarg, J. 1994. Transport properties of single-file pores with two conformational states. *Biophys. J.* **67:**996–1006

Hill, T.L. 1977. Free Energy Transduction in Biology. Academic Press, New York

Hill, T.L. 1989. Free Energy Transduction and Biochemical Cycle Kinetics. Springer-Verlag, New York

Holman, G.D. 1980. An allosteric pore model for sugar transport in human erythrocytes. *Biochim. Biophys. Acta* **599:**202–213

Jung, E.K.Y., Chin, J.J., Jung, C.Y. 1986. Structural basis of human erythrocyte glucose transporter function in reconstituted system. Hydrogen exchange. *J. Biol. Chem.* **261:**9155–9160

Krupka, R.M. 1972. Combined effects of maltose and deoxyglucose on fluorodinitrobenzene inactivation of sugar transport in erythrocytes. *Biochim. Biophys. Acta* **282:**326–336

Krupka, R.M. 1989. Testing transport models and transport data by means of kinetic rejection criteria. *Biochem. J.* **260:**885–891

Krupka, R.M., Deves, R. 1981. An experimental test for cyclic versus linear transport models. The mechanism of glucose and choline transport in erythrocytes. *J. Biol. Chem.* **256:**5410–5416

Krupka, R.M., Deves, R. 1983. Kinetics of inhibition of transport systems. *Int. Rev. Cytol.* **84:**303–352

Lacko, L., Wittke, B., Geck, P. 1973. The temperature dependence of the exchange transport of glucose in human erythrocytes. *J. Cell. Physiol.* **82:**213–218

Läuger, P. 1980. Kinetic properties of ion carriers and channels. *J. Membrane Biol.* **57:**163–178

Läuger, P. 1984. Channels with multiple conformational states: interrelations with carriers and pumps. *In:* Current Topics in Membrane and Transport. F. Bronner and W.D. Stein, Editors **21:**309–326. Academic, New York

Lieb, W.R. 1982. A kinetic approach to transport studies. *In:* Red Cell Membranes: A Methodological Approach. J.C. Ellory and J.D. Young, Editors pp. 135–164. Academic, New York

Lieb, W.R., Stein, W.D. 1970. Quantitative predictions of a noncarrier model for glucose transport across the human red cell membrane. *Biophys. J.* **10:**585–605

Lieb, W.R., Stein, W.D. 1974. Testing and characterizing the simple carrier. *Biochim. Biophys. Acta* **373:**178–196

Lowe, A.G., Walmsley, A.R. 1986. The kinetics of glucose transport in human red blood cells. *Biochim. Biophys. Acta* **857:**146–154

Marshall, B.A., Murata, H., Hresko, R.C., Mueckler, M. Domains that confer intracellular sequestration of the GLUT4 glucose transporter in *Xenopus* oocytes. *J. Biol. Chem.* **268:**26193–26199

Mueckler, M. 1994. Facilitative glucose transporters. *Eur. J. Biochem.* **219:**713–725

Mueckler, M., Caruso, C., Baldwin, S.A., Panico, M., Blench, I., Morris, H.R., Allard, W.J., Lienhard, G.E., Lodish, H.F. 1985. Sequence and structure of a human glucose transporter. *Science* **229:**941–945

Naftalin, R.J. 1970. A model for sugar transport across red cell membranes without carriers. *Biochim. Biophys. Acta* **211:**65–78

Naftalin, R.J., Smith, P.M., Roselaar, S.E. 1985. Evidence for non-uniform distribution of D-glucose within human red cells during net exit and counterflow. *Biochim. Biophys. Acta* **820:**235–249

Pessino, A., Hebert, D.N., Woon, C.W., Harrison, S.A., Clancey, B.M., Buxton, J.M., Carruthers, A., Czech, M.P. 1991. Evidence that functional erythrocyte-type glucose transporters are oligomers. *J. Biol. Chem.* **266:**20213–20217

Shetty, M., Loeb, J.N., Vikstrom, K., Ismail-Beigi, F. 1993. Rapid activation of GLUT-1 glucose transporter following inhibition of

oxidative phosphorylation in Clone 9 cells. *J. Biol. Chem.* **268:** 17225–17232

Sofue, M., Yoshimura, Y., Nishida, M., Kawada, J. 1992. Possible multifunction of glucose transporter. Transport of nicotinamide by reconstituted liposomes. *Biochem. J.* **288:**669–674

Stein, W.D. 1986. Transport and Diffusion across Cell Membranes. Academic Press, Orlando, FL

Vera, J.C., Rivas, C.I., Fischbarg, J., Golde, D.W. 1993. Mammalian facilitative hexose transporters mediate the transport of dehydroascorbic acid. *Nature* **364:**79–82

Walmsley, A.R. 1988. The dynamics of the glucose transporter. *Trends Biochem. Sci.* **13:**226–231

Walmsley, A.R., Martin, G.E.M., McDonald, T.P., Henderson, P.J.F. 1994. The presteady-state kinetics of conformational changes in sugar transporters. *Biochem. Soc. Trans.* **22:**650–654

Weiser, M.B., Razin, M., Stein, W.D. 1983. Kinetic tests of models for sugar transport in human erythrocytes and a comparison of fresh and cold-stored cells. *Biochim. Biophys. Acta* **727:**379–388

Wheeler, T.J. 1986. Kinetics of glucose transport in human erythrocyte: zero-trans efflux and infinite-trans efflux at 0°C. *Biochim. Biophys. Acta* **862:**387–398

Wheeler, T.J., Hinkle, P.C. 1985. The glucose transporter of mammalian cells. *Ann. Rev. Physiol.* **47:**503–517

Wheeler, T.J., Wheelan, T.D. 1988. Infinite-cis kinetics support the carrier model for erythrocyte glucose transport. *Biochemistry* **27:**1441–1450

Widdas, W.F. 1952. Inability of diffusion to account for placental glucose transfer in the sheep and consideration of the kinetics of a possible carrier transfer. *J. Physiol.* **118:**23–39

Zhang, R., Alper, S.L., Thorens, B., Verkman, A.S. 1991. Evidence from oocyte expression that the erythrocyte water channel is distinct from band 3 and the glucose transporter. *J. Clin. Invest.* **88:**1553–1558

Appendix I

Steady-state Analysis of the Single-occupancy Model

We perform here the steady-state analysis of the model corresponding to the single-occupancy limit of the diagram of Fig. 1*A*, employing the method derived by Hill (1977). For the analysis, we consider that N is the total amount of transporters (for instance, expressed as a density, in mole/cm^2), and that S_1 and S_2 are the activities of the transported ligand in compartments 1 and 2 respectively. As it is shown in Fig. 1*A*, b_1, b_2, r_1, r_2, k_1, k_{-1}, l_1, l_{-1}, α_1, α_{-1}, β_1, and β_{-1}, are the rate constants governing the kinetics. Since only cycles *a* and *b* (Fig. 1*B*) result in net transport of S (J_S), taking the 1 to 2 direction as positive, is given by

$$J_S = (N/\Sigma)\,(\Pi_a\Sigma_a + \Pi_b\Sigma_b)\,(S_1 - S_2) \tag{A1}$$

where, under the restriction of detailed balance,

$$\begin{aligned}\Pi_a &= b_1k_1\beta_1r_2\alpha_{-1} = b_2k_{-1}\beta_{-1}r_1\alpha_1\\ \Pi_b &= b_1l_1\beta_1r_2\alpha_{-1} = b_2l_{-1}\beta_{-1}r_1\alpha_1\end{aligned} \tag{A2}$$

and where Σ_a and Σ_b are given by

$$\Sigma_a = l_1 + \beta_{-1};\ \Sigma_b = k_{-1} + \beta_1 \tag{A3}$$

The denominator Σ is the sum of all the directional diagrams corresponding to the single-occupancy portion only of the complete model of Fig. 1*A*, and is given by

$$\Sigma = D_E + D_{E'} + D_Y + D_{Y'} + D_X + D_{X'} \tag{A4}$$

where $D_i (i = E, E', Y, Y', X, X')$ is the directional diagram of the ith state of the transporter, given by

$$\begin{aligned}D_E &= \alpha_{-1}r_2D_{Y'}{}^c + (b_2S_2 + \alpha_{-1})r_1D_Y{}^c + \alpha_{-1}r_1r_2(l_1 + \beta_{-1})(k_{-1} + \beta_1)\\ D_{E'} &= \alpha_1r_1D_Y{}^c + (b_1S_1 + \alpha_1)r_2D_{Y'}{}^c + \alpha_1r_1r_2(l_1 + \beta_{-1})(k_{-1} + \beta_1)\\ D_Y &= (\alpha_{-1}b_1S_1 + \alpha_1b_2S_2 + b_1b_2S_1S_2)D_Y{}^c + r_2\alpha_{-1}b_1S_1(l_1 + \beta_{-1})(k_{-1} + \beta_1)\\ D_{Y'} &= (\alpha_{-1}b_1S_1 + \alpha_1b_2S_2 + b_1b_2S_1S_2)D_{Y'}{}^c + r_1\alpha_1b_2S_2(l_1 + \beta_{-1})(k_{-1} + \beta_1)\\ D_X &= (\alpha_{-1}b_1S_1 + \alpha_1b_2S_2 + b_1b_2S_1S_2)D_X{}^c + (k_1r_2\alpha_{-1}b_1S_1 + \beta_{-1}r_1\alpha_1b_2S_2)\\ &\quad (l_1 + \beta_{-1})\\ D_{X'} &= (\alpha_{-1}b_1S_1 + \alpha_1b_2S_2 + b_1b_2S_1S_2)D_{X'}{}^c + (\beta_1r_2\alpha_{-1}b_1S_1\\ &\quad + l_{-1}r_1\alpha_1b_2S_2)(k_{-1} + \beta_1)\end{aligned} \tag{A5}$$

In these expressions, $D_Y{}^c$, $D_{Y'}{}^c$, $D_X{}^c$, and $D_{X'}{}^c$ are the directional diagrams of the corresponding states for cycle *c* only, and are given by

$$\begin{aligned}D_Y{}^c &= \beta_{-1}[l_{-1}\,(k_{-1} + \beta_1) + k_{-1}(l_1 + \beta_{-1})]\\ D_{Y'}{}^c &= \beta_1[l_1(k_{-1} + \beta_1) + k_1(l_1 + \beta_{-1})]\\ D_X{}^c &= \beta_{-1}[k_1(l_1 + \beta_{-1}) + \beta_1l_1 + k_1l_{-1}]\\ D_{X'}{}^c &= \beta_1[l_{-1}(k_{-1} + \beta_1) + \beta_{-1}k_{-1} + k_1l_{-1}]\end{aligned} \tag{A6}$$

Therefore, for the situation analyzed in this section, the steady-state density N_i of the *i*th state of the transporter is given by $N_i = ND_i/\Sigma$.

The unidirectional fluxes of S in the $1 \rightarrow 2$ and $2 \rightarrow 1$ directions (v_{12} and v_{21} respectively) can be derived either by employing the methods proposed by Britton (1977), or from the cyclic diagrams shown in Figs. 3*A* and 3*B*. From the analysis, v_{12} and v_{21} are given by

$$v_{12} = [N(\Pi_a\Sigma_a + \Pi_b\Sigma_b)S_1/\Sigma]\,(D_E/\alpha_{-1}D_u) \tag{A7a}$$

$$v_{21} = [N(\Pi_a\Sigma_a + \Pi_b\Sigma_b)S_2/\Sigma]\,(D_{E'}/\alpha_1D_u) \tag{A7b}$$

where $\alpha_{-1}D_u$ (α_1D_u) is the sum of all the directional diagrams of state E (E') in the diagram of Fig. 3*A* (3*B*), that contain step α_{-1} (α_1). Hence

$$D_u = r_1D_Y{}^c + r_2D_{Y'}{}^c + r_1r_2(l_1 + \beta_{-1})(k_{-1} + \beta_1) \tag{A8}$$

From Eqs. (A5) and (A8), we can express D_E and $D_{E'}$ as

$$\begin{aligned}D_E &= \alpha_{-1}D_u + r_1b_2D_{Y'}{}^cS_2;\\ D_{E'} &= \alpha_1D_u + r_2b_1D_Y{}^cS_1\end{aligned} \tag{A9}$$

Eqs. (A7)–(A9) and the condition of detailed balance [Eq. (A2)] can be employed to demonstrate that, as required,

$$J_S = v_{12} - v_{21} \tag{A10}$$

The unidirectional fluxes v_{12} and v_{21} can also be expressed as

$$v_{12} = (T_1S_1 + T_3S_1S_2)/E_0 + E_1S_1 + E_2S_2 + E_3S_1S_2) \tag{A11a}$$

$$v_{21} = (T_2S_2 + T_3S_1S_2)/(E_0 + E_1S_1 + E_2S_2 + E_3S_1S_2) \tag{A11b}$$

where, from Eqs. (A4)–(A10),

$$\begin{aligned}T_1 &= T_2 = N(\Pi_a\Sigma_a + \Pi_b\Sigma_b)\\ T_3 &= (T_1/D_u)(r_1b_2D_Y{}^c/\alpha_{-1}) = (T_1/D_u)(r_2b_1D_{Y'}{}^c/\alpha_1)\\ E_0 &= (\alpha_1 + \alpha_{-1})[r_1D_Y{}^c + r_2D_{Y'}{}^c + r_1r_2(l_1 + \beta_{-1})(k_{-1} + \beta_1)]\\ E_1 &= b_1\{r_2D_{Y'}{}^c + \alpha_{-1}(D_Y{}^c + D_{Y'}{}^c + D_X{}^c + D_{X'}{}^c) + \alpha_{-1}r_2[(l_1 + \beta_{-1})(k_{-1}\end{aligned}$$

$$+ \beta_1) + k_1(l_1 + \beta_{-1}) + \beta_1(k_{-1} + \beta_1)]\}$$

$$E_2 = b_2\{r_1 D_Y{}^c + \alpha_1(D_Y{}^c + D_{Y'}{}^c + D_X{}^c + D_{X'}{}^c) + \alpha_1 r_1[(l_1 + \beta_{-1})(k_{-1} + \beta_1) + \beta_{-1}(l_1 + \beta_{-1}) + l_{-1}(k_{-1} + \beta_1)]\}$$

$$E_3 = (D_Y{}^c + D_{Y'}{}^c + D_X{}^c + D_{X'}{}^c)b_1 b_2 \quad \text{(A12)}$$

Besides the condition of detailed balance, transport models of the type of Fig. 1*A* are also subject to kinetic restrictions. For the case of the single-occupancy limit, it can be demonstrated that

$$E_1 + E_2 = E_0 T_3/T_1 + E_3 T_1/T_3 \quad \text{(A13)}$$

The unidirectional fluxes can also be expressed as functions of the relevant experimental parameters K, R_{12}, R_{21}, R_{00} and R_{ee} (Lieb & Stein, 1974; Stein, 1986, pp. 237–242). The following definitions relate them to the factors expressed by Eqs. (A12):

$$K = T_1/T_3;\ KR_{00} = E_0/T_1;$$
$$R_{12} = E_1/T_1;\ R_{21} = E_2/T_1, \text{ and } R_{ee}/K = E_3/T_1 \quad \text{(A14)}$$

Appendix II

Some General Considerations About the Complete Model (Fig. 1A). Steady-state Analysis of the Model Represented by Cycle *g* (Fig. 1B)

We offer here some general considerations about the complete model of Fig. 1*A*, and then perform the detailed steady-state analysis of the model represented by cycle *g* only (Fig. 1*B*), using as before the method developed by Hill (1977). Superindexes ''cm'' and ''dbl'' indicate parameters corresponding to the mode of operation of the complete model and the double-occupancy limit, respectively. Superindex ''*g*'' indicates parameters corresponding to cycle *g* only. Absence of superindex indicates the mode of operation of the single-occupancy limit (*see* Appendix I). Besides the rate constants considered in Appendix I, the constants f_1, f_2, g_1, g_2, γ_1 and γ_{-1} govern the kinetics. A particular case of the model would be given, for example, by the condition $b_1 = f_1$, $b_2 = f_2$, $r_1 = g_1$, $r_2 = g_2$, $\alpha_1 = \beta_1 = \gamma_1$, and $\alpha_{-1} = \beta_{-1} = \gamma_{-1}$, that would imply that both the binding and release of ligand molecules, and the conformational transitions, are not affected by the occupancy state of the transporter.

For the complete model of Fig. 1*A*, the movement of *S* between compartment 1 and 2 is determined by cycles *a*, *b*, *d*, *e* and *g* (Fig. 1*B*). The net flux $J_S{}^{cm}$ is therefore given by

$$J_S{}^{cm} = J_a{}^{cm} + J_b{}^{cm} + J_d{}^{cm} + J_e{}^{cm} + 2J_g{}^{cm} \quad \text{(A15)}$$

where $J_a{}^{cm}$, $J_b{}^{cm}$, $J_d{}^{cm}$, $J_e{}^{cm}$, and $J_g{}^{cm}$ are the corresponding cycle fluxes taken positive, for instance, in the counterclockwise direction.

There are two limiting behaviors of the model, that correspond to the single and double occupancy regimes respectively. It can be demonstrated that the necessary condition for the single-occupancy limit is

$$r_1, r_2 \gg b_1 S_1, b_2 S_2 \text{ and } g_1, g_2 \gg f_1 S_1, f_2 S_2 \quad \text{(A16)}$$

Under this condition, the model becomes the one analyzed in Appendix I. Correspondingly, it can be demonstrated that the net flux $J_S{}^{cm}$ [given by Eq. (A15)] becomes J_S [given by Eq. (A1)].

Analogously, it can be demonstrated that the necessary condition for the double-occupancy limit is

$$b_1 S_1, b_2 S_2 \gg r_1, r_2 \text{ and } f_1 S_1, f_2 S_2 \gg g_1, g_2 \quad \text{(A17)}$$

Under this condition, only cycles *e* and *d* are significantly determining ligand transport. Thus, the net flux $J_S{}^{cm}$ [Eq. (A15)] now becomes $J_S{}^{dbl}$, given by

$$J_S{}^{dbl} = J_d{}^{dbl} + J_e{}^{dbl} \quad \text{(A18)}$$

Under any condition intermediate between those corresponding to (A16)and (A17), the complete model of Fig. 1*A* has to be invoked. For some interval of the ligand activities, cycle *g* could approximately represent the average mode of operation of the model. One necessary condition to fulfill this situation would be that $f_1 S_1 \gg \beta_1$ and $f_2 S_2 \gg \beta_{-1}$ simultaneously. We now proceed to derive explicit expressions for the net and unidirectional fluxes determined by this cycle. The net flux of *S* determined by cycle *g* only, $J_S{}^g$, is given by

$$J_S{}^g = 2J_g \quad \text{(A19)}$$

where J_g represents the cycle flux of cycle *g* functioning separately, and is in turn given by

$$J_g = (N/\Sigma_g)\Pi_g(S_1 - S_2) \quad \text{(A20)}$$

In Eq. (A20) Σ_g is the sum of all the directional diagrams of all the states for cycle *g* only:

$$\Sigma_g = D_E{}^g + D_{E'}{}^g + D_Y{}^g + D_{Y'}{}^g + D_X{}^g + D_{X'}{}^g + D_C{}^g + D_{C'}{}^g \quad \text{(A21)}$$

where

$$D_E{}^g = \alpha_{-1}k_{-1}l_1 r_1 r_2 G + \alpha_{-1}\gamma_1 g_2 l_1 r_2(k_1 + r_1)f_1 S_1 + \alpha_{-1}\gamma_{-1}g_1 k_{-1} r_1(l_{-1} + r_2)f_2 S_2 + \gamma_{-1}g_1 k_{-1} l_{-1} r_1 b_2 f_2 S_2{}^2$$

$$D_{E'}{}^g = \alpha_1 k_{-1} l_1 r_1 r_2 G + \alpha_1\gamma_1 g_2 l_1 r_2(k_1 + r_1)f_1 S_1 + \alpha_1\gamma_{-1}g_1 k_{-1} r_1(l_{-1} + r_2)f_2 S_2 + \gamma_1 g_2 k_1 l_1 r_2 b_1 f_1 S_1{}^2$$

$$D_Y{}^g = \alpha_{-1}k_{-1}l_1 r_2 G b_1 S_1 + \alpha_{-1}\gamma_{-1}g_1 k_{-1}(l_{-1} + r_2)b_1 f_2 S_1 S_2 + \alpha_{-1}\gamma_1 g_2 l_1 r_2 b_1 f_1 S_1{}^2 + \alpha_1\gamma_{-1}g_1 k_{-1} l_{-1} b_2 f_2 S_2{}^2 + \gamma_{-1}g_1 k_{-1} l_{-1} b_1 b_2 f_2 S_1 S_2{}^2$$

$$D_{Y'}{}^g = \alpha_1 k_{-1} l_1 r_1 G b_2 S_2 + \alpha_1\gamma_1 g_2 l_1(k_1 + r_1)b_2 f_1 S_1 S_2 + \alpha_1\gamma_{-1}g_1 k_{-1} r_1 b_2 f_2 S_2{}^2 + \alpha_{-1}\gamma_1 g_2 k_1 l_1 b_1 f_1 S_1{}^2 + \gamma_1 g_2 k_1 l_1 b_1 b_2 f_1 S_1{}^2 S_2$$

$$D_X{}^g = \alpha_{-1}k_1 l_1 r_2 G b_1 S_1 + \alpha_1\gamma_{-1}g_1 l_{-1}(k_1 + r_1)b_2 f_2 S_2{}^2 + \alpha_{-1}\gamma_{-1}g_1 k_1(l_{-1} + r_2)b_1 f_2 S_1 S_2 + \gamma_{-1}g_1 k_1 l_{-1} b_1 b_2 f_2 S_1 S_2{}^2$$

$$D_{X'}{}^g = \alpha_1 k_{-1} l_{-1} r_1 G b_2 S_2 + \alpha_1\gamma_1 g_2 l_{-1}(k_1 + r_1)\ b_2 f_1 S_1 S_2 + \alpha_{-1}\gamma_1 g_2 k_1(l_{-1} + r_2)b_1 f_1 S_1{}^2 + \gamma_1 g_2 k_1 l_{-1} b_1 b_2 f_1 S_1{}^2 S_2$$

$$D_C{}^g = \alpha_{-1}k_1 l_1 r_2(\gamma_{-1} + g_2)b_1 f_1 S_1{}^2 + \alpha_1\gamma_{-1}l_{-1}(k_1 + r_1)b_2 f_1 f_2 S_1 S_2{}^2 + \alpha_1\gamma_{-1}k_{-1}l_{-1}r_1 b_2 f_2 S_2{}^2 + \alpha_{-1}\gamma_{-1}k_1(l_{-1} + r_2)b_1 f_1 f_2 S_1{}^2 S_2 + \gamma_{-1}k_1 l_{-1} b_1 b_2 f_1 f_2 S_1{}^2 S_2{}^2$$

$$D_{C'}{}^g = \alpha_1 k_{-1} l_{-1} r_1(\gamma_1 + g_1)b_2 f_2 S_2{}^2 + \alpha_1\gamma_1 l_{-1}(k_1 + r_1)b_2 f_1 f_2 S_1 S_2{}^2 + \alpha_{-1}\gamma_1 k_1 l_1 r_2 b_1 f_1 S_1{}^2 + \alpha_{-1}\gamma_1 k_1(l_{-1} + r_2)b_1 f_1 f_2 S_1{}^2 S_2 + \gamma_1 k_1 l_{-1} b_1 b_2 f_1 f_2 S_1{}^2 S_2{}^2 \quad \text{(A22)}$$

with $G = \gamma_1 g_2 + \gamma_{-1} g_1 + g_1 g_2$.

For the case represented by cycle *g* only, the steady-state density $N_i{}^g$ of the *i*th state is therefore given by $N_i{}^g = N\ D_i{}^g/\Sigma_g$.

From Eqs. (A21)–(A22) we notice that Σ_g can also be expressed by

$$\Sigma_g = H_0 + H_1 S_1 + H_2 S_2 + H_3 S_1 S_2 + H_4 S_1{}^2 + H_5 S_2{}^2 + H_6 S_1{}^2 S_2 + H_7 S_1 S_2{}^2 + H_8 S_1{}^2 S_2{}^2 \quad \text{(A23)}$$

where the *H*'s are functions of the rate constants and are independent of the ligand activities.

In Eq. (A20) detailed balance requires that

$$\Pi_g = b_1 k_1 f_1 \gamma_1 g_2 l_1 r_2 \alpha_{-1} = b_2 l_{-1} f_2 \gamma_{-1} g_1 k_{-1} r_1 \alpha_1 \quad \text{(A24)}$$

Figure 4*A* and *B* show the cyclic diagrams corresponding to cycle *g* that can be used to derive the expressions for the unidirectional fluxes of *S*. By using the schemes shown in these figures it can be seen that, considering for instance that 1 to 2 direction, a molecule of *S* will be released at step $C' \rightarrow X'$ if bound by state *E*, and at step $Y' \rightarrow E'$ if bound by state *X*. Therefore, the total unidirectional fluxes ${v_{12}}^g$ and ${v_{21}}^g$ in the $1 \rightarrow 2$ and $2 \rightarrow 1$ directions respectively, are given by

$$ {v_{12}}^g = {v_{12}}^E + {v_{12}}^X \tag{A25a} $$

$$ {v_{21}}^g = {v_{21}}^{E'} + {v_{21}}^{X'} \tag{A25b} $$

where

$$ \begin{aligned} {v_{12}}^E &= (N\Pi_g/\Sigma_g)[({S_1}^2 {D_E}^g)/(\alpha_{-1} l_1 r_2 {D_u}^g)] \\ {v_{12}}^X &= (N\Pi_g/\Sigma_g)[({S_1}^2 {D_X}^g)/(\alpha_{-1} k_1 b_1 S_1 {D_u}^{g'})] \\ {v_{21}}^{E'} &= (N\Pi_g/\Sigma_g)[({S_2}^2 {D_{E'}}^g)/(\alpha_1 k_{-1} r_1 {D_u}^{g'})] \\ {v_{21}}^{X'} &= (N\Pi_g/\Sigma_g)[({S_2}^2 {D_{X'}}^g)/(\alpha_{-1} l_1 r_2 {D_u}^g)] \end{aligned} \tag{A26} $$

with ${D_u}^g = k_{-1} r_1 G = \gamma_1 g_2 (k_1 + r_1) f_1 S_1$ and ${D_u}^{g'} = l_1 r_2 G + \gamma_{-1} g_1 (l_{-1} + r_2) f_2 S_2$. Eqs. (A25)–(A26) and the condition of detailed balance [Eq. (A24)] can be employed to demonstrate that, as required,

$$ {v_{12}}^E - {v_{21}}^{X'} = {v_{12}}^X - {v_{21}}^{E'} = J_g \tag{A27} $$

Kinetic restrictions analogous to the one represented by Eq. (A13) for the particular case of the single-occupancy limit may apply to the model represented by the cycle *g* only, but they are not analyzed here.

Appendix III

A Numerical Example

Our objective here is to calculate values for the apparent K_ms and maximum velocities for the model of Fig. 1*A* under different experiment conditions. We do this for both the single-occupancy regime and cycle *g*. We compute a particular set of numerical values for the rate constants (*see below*); subindices 1 and 2 denote intra and extracellular compartments, respectively. The rate constants we computed are:

$b_1 = 6 \times 10^5$ cm^3 mmol^{-1} s^{-1}; $b_2 = 6 \times 10^5$ cm^3 mmol^{-1} s^{-1};
$r_1 = 1.5 \times 10^4$ s^{-1}; $r_2 = 6 \times 10^3$ s^{-1};
$k_1 = 2 \times 10^3$ s^{-1}; $k_{-1} = 1081.761$ s^{-1};
$l_1 = 2 \times 10^3$ s^{-1}; $l_{-1} = 1081.761$ s^{-1};
$\alpha_1 = 0.726$ s^{-1}; $\alpha_{-1} = 12.1$ s^{-1};
$\beta_1 = 90.3$ s^{-1}; $\beta_{-1} = 1113$ s^{-1};
$f_1 = 3 \times 10^6$ cm^3 mmol^{-1} s^{-1}; $f_2 = 3 \times 10^6$ cm^3 mmol^{-1} s^{-1};
$g_1 = 1 \times 10^4$ s^{-1}; $g_2 = 5408.806$ s^{-1};
$\gamma_1 = 90.3$ s^{-1}; $\gamma_{-1} = 1113$ s^{-1}.

The values for the rate constants governing the conformational transitions between the empty and occupied states of the transporter were taken from Lowe and Walmsley (1986). The values for rest of the rate constants were determined heuristically by trial-and-error so as to fit all the experimental data; of course, given the large number of rate constants governing the system, the set of values obtained in such manner may not be unique. For the values shown above, the equilibrium dissociation constants at the inner and outer binding sites are $K_d(\text{in}) = r_1/b_1 = 25$ mM and $K_d(\text{out}) = r_2/b_2 = 10$ mM respectively, in agreement with experimental evidence (Baldwin, 1993). The rate constants k_{-1} and l_{-1}, and g_2, were imposed by the conditions of detailed balance expressed by Eqs. (A2) and (A24) respectively.

The total density of the transporter was set at $N = 5 \times 10^{-10}$ mmol cm^{-2}; assuming a surface area *A* of 1.4×10^{-6} cm^2 for a human erythrocyte, such density represents approximately 5×10^5 GLUT1 copies per cell (*see* Baldwin, 1993). With these units, the ligand fluxes are expressed in mmol cm^{-2} s^{-1}. Since most experiments determine variations in ligand concentration per unit time, a conversion factor appears. Thus, for instance, if J_s is the net ligand flux (in mmol cm^{-2} s^{-1}) considered positive in the $2 \rightarrow 1$ direction, the variation in the intracellular concentration S_1 will be given by $dS_1/dt = (A/V)J_s$. Here, *V* is the volume of the human erythrocyte, which we take to be 9×10^{-11} cm^3.

Table 2 shows values calculated for the kinetic parameters corresponding to the single-occupancy mode of Fig. 1*A* with the rate constant values above. The experimentally relevant parameters were determined using equations (A12)–(A14). These parameters were in turn used to obtain the values for the maximal velocities and apparent K_ms shown in the lower portion of that table.

Figure 5 shows the dependence of the ligand fluxes on the corresponding ligand concentrations under infinite-cis and infinite-trans conditions, using the rate constants above in the expressions for cycle *g*. Figure 5*A* (efflux in Eq. (3) as a function of S_2) describes efflux under infinite-cis conditions (that is, saturating S_1). Analogously, Fig. 5*B* corresponds to influx under infinite-cis conditions (e.g., saturating S_2). Figure 5*C* (efflux in Eq. (5) as a function of S_1) describes ligand efflux under infinite-trans conditions (saturating S_2). Lastly, Fig. 5*D* describes influx under infinite-trans conditions (saturating S_1). The maximal velocities and apparent K_m values for these fluxes were obtained from the respective curves (*see* Fig. 5 legend and Table 3).

Table 3 shows the maximal velocities and apparent K_ms under infinite-cis and infinite-trans conditions obtained for: (*a*) the single occupancy regime using the experimentally relevant parameters (Stein, 1986, pp. 237–242) listed in Table 2; (*b*) for cycle *g* only (derived in Fig. 5); and (*c*) actual experiments.